STRUCTURAL RESPONSE OF FAST-REACTOR CORE SUBASSEMBLIES TO THERMAL LOADING

R.F. KULAK, J.M. KENNEDY

Reactor Analysis and Safety Division,
Argonne National Laboratory, Argonne, Illinois 60439 U.S.A.

T. BELYTSCHKO

Department of Materials Engineering,
University of Illinois at Chicago, Chicago, Illinois 60680 U.S.A.

SUMMARY

When evaluating the safety aspects of reactor components, such as core subassemblies, thermal stress analysis is necessary to predict possible failure or failure propagation when components are subjected to high heat fluxes. With this consideration the three-dimensional structural response of a hexagonal fuel assembly duct to severe thermal loading is studied. The purpose of this analysis is to predict thermal stresses during a subassembly-to-subassembly failure propagation event. During this event the accident subassembly would deposit molten fuel on an adjacent subassembly duct which would set up high thermal stresses along a portion of one flat.

In order to determine the structural behavior of a thermally loaded hexcan, the stiffness matrix method of structural mechanics is incorporated into SADCAT (see A. H. Marchertas and T.B. Belyttschko, "Nonlinear Finite-element Formulation for Transient Analysis of Three-dimensional Thin Structures", Argonne National Laboratory Report ANL-8104) a finite element code developed at Argonne National Laboratory. The temperature profile across the inner and outer surface of the structure is interpolated from the inner and outer nodal temperatures.

The thermal loads are determined in the following manner. First, the thermal stresses in each element are computed using the element nodal temperatures and material properties. Next, the local thermal internal nodal loads are determined from the thermal stresses. Then the local thermal loads are assembled into global thermal loads which are then treated as external nodal loads. Since geometric nonlinearity (i.e., those characterized by large rotations and small strains) and material nonlinearity (elasto-plastic behavior) are accounted for, the computational procedure followed was an incremental linearization technique with energy balance checks.

The structural response of a Liquid Metal Fast Breeder Reactor (LMFBR) hexcan when a high heat flux is applied to the outside of one flat is presented. Results for hexcan displacements and internal stress distributions are presented for both unirradiated and irradiated duct material. A comparison is made between duct wall response as predicted from a plane stress and plane strain two-dimensional analysis and the behavior as predicted by a three-dimensional analysis. It is found that for a given reference temperature and yield strength there is a limit to the maximum temperature difference through the duct wall which can be tolerated by the heated zone before buckling or wrinkling occurred.

1. Introduction

One of the important functions of the subassembly in the Liquid Metal Fast Breeder Reactor (LMFBR) core is to contain disruptions and accidents. Beyltschko, et al, [1] have investigated the structural response of hexcans due to impulsive pressure loadings arising from either (1) a molten fuel-coolant interaction (MFCI) or (2) fission gas release. Another type of loading which has become the subject of considerable interest in the safety analysis of the LMFBR is thermal loading on subassemblies adjacent to accident subassemblies (fig. 1). Crawford, et al, [2] state that large temperature gradients through the duct wall may arise (1) with the deposition of molten fuel on the hexcan wall and (2) when local boiling of the sodium occurs adjacent to the wall. For example, in the model development for the subassembly-to-subassembly failure propagation event, it is hypothesized that the duct wall of an accident subassembly fails and deposits molten fuel on the outer wall of an adjacent subassembly. In order to determine if the deposited fuel will fail the adjacent wall and thus propagate the event, a thermal stress analysis is necessary.

In conjunction with the analytical investigation of this problem, an out-of-pile meltthrough test is presently being prepared. Upon completion, the experimental results will be used in conjunction with code studies to evaluate the safety of thermally loaded subassemblies.

The purposes of the present analysis are (1) to determine the structural response of the duct wall when a high heat flux is applied to the outside of one flat, (2) to gain insight into the physical phenomena of a thermally loaded hexcan, and (3) to provide response data for corroboration with experimental studies.

2. Method of Analysis

During the meltthrough test, a heat flux is applied to a single flat of a hexagonal duct over a zone 2.5 in. wide and 12 in. long (fig. 2). The inside and outside wall temperatures within the heated zone are assumed to be uniform at values T_i and T_o, respectively. The temperature variation through the wall is assumed to be linear; this is not necessary in the analysis but was done for convenience. Outside the heated zone, temperature gradients are assumed not to exist.

In this study the above problem will be investigated by considering two models: a thin ring model and a plate model. The ring model is analyzed using the computer code STRAW [3] which is a two-dimensional finite-element code capable of treating both material and geometric nonlinearities. The thermally loaded hexcan is modeled by considering a thin slice of the hexcan at midlength of the heated zone (fig. 2). Because of symmetry in duct geometry and thermal loading, only one-half of the duct is modeled. The finite element model used in the STRAW code is shown in fig. 3. The following boundary conditions are imposed:

Point A $U_y = 0, \theta_z = 0$

Point E $U_x = U_y = 0, \theta_z = 0$

where U_x and U_y are the displacements in the x and y directions and θ_z is the rotation about the z-axis. Flat AB is thermally loaded while flats BC, CD, and DE are maintained at a uniform temperature.

A problem associated with severe heating of a portion of a hexcan is the wrinkling which occurs in the heated zone. In order to study this phenomena, a plate model which consists only of the 12 x 2.5 in. heated zone (see fig. 3) was constructed. This model is analyzed using SADCAT [4], a finite element plate/shell code developed at Argonne National

Laboratory. Because of geometric and loading symmetry, only one-half of the heated zone was modeled. The finite element mesh (fig. 4) consists of 144 triangular plate elements. The boundaries of the plate are fixed. It is noted that these boundary conditions overrepresent the rigidity of the unheated portion of the hexcan.

The stiffness matrix method (see for example, Zienkiewicz [5]) is used to determine the response of a thermally loaded hexcan. The computational procedure utilized is an incremental linearization technique with energy balance checks. Thus, geometric nonlinearity (i.e., those characterized by large rotations and small strain) and material nonlinearity (elasto-plastic behavior) can be handled. The thermal loading is treated in the following manner. The thermal stresses in each finite element are computed based upon the material properties and the nodal temperatures within that element. Next, the local thermal internal nodal load matrix is computed from the element thermal stresses. The local thermal load matrix for each element is assembled into the global thermal load matrix which in turn is treated as an external load matrix.

3. Material Properties and Models

The variation in material property data with temperature used herein is tabulated in Table I. Because no data could be located for the material properties at the higher temperatures, the data from ref. [6] is extrapolated. Since 316 stainless steel exhibits large variations in yield stress with temperature, it was accounted for in the code.

The temperature dependent stress-strain curve (fig. 5) for duct material is taken to be elastic-strain hardening plastic in which the Young's and tangent modulii are assumed to be temperature independent. Because Young's modulus did not vary greatly within the temperature range considered, its value is taken to be constant 20×10^6 psi; the tangent modulus is taken to be 1×10^6 psi.

Although a plane stress analysis is the simplest approach to this problem the results predicted will tend to be nonconservative (i.e., on the unsafe side). In order to account for a two-dimensional state of stress, such as that existing in a hexcan, an approximate formulation was developed for thermo-elasto-plastic plane strain, similar to the approximate plane strain elastic-plastic relations developed in [1].

The thermo-elastic two-dimensional stress-strain relationship for zero shear strain are

$$\begin{Bmatrix} \sigma_x \\ \sigma_y \end{Bmatrix} = \frac{E}{1-\nu^2} \begin{bmatrix} 1 & \nu \\ \nu & 1 \end{bmatrix} \begin{Bmatrix} \varepsilon_x \\ \varepsilon_y \end{Bmatrix} - \frac{E\alpha T}{1-\nu} \begin{Bmatrix} 1 \\ 1 \end{Bmatrix} \qquad (1)$$

where

σ_x, σ_y - stresses in circumferential and axial direction, respectively

$\varepsilon_x, \varepsilon_y$ - strains in circumferential and axial direction, respectively

T - temperature difference

E - Young's modulus

ν - Poisson's ratio

α - linear coefficient of thermal expansion

For the case of plane strain, ε_y is zero and σ_y , as determined from (1) is given below

$$\sigma_y = \nu\sigma_x - \alpha ET \qquad (2)$$

$$\sigma_o^2 = \frac{1}{2}\left[(\sigma_x - \sigma_y)^2 + \sigma_y^2 + \sigma_x^2\right] \tag{3}$$

where σ_o is the yield stress in simple tension. Substitution of eq. (2) into (3) gives the following yield condition

$$\sigma_o^2 = C_1\,\sigma_x^2 + C_2\,\sigma_x T + C_3\,T^2 \tag{4}$$

where

$$C_1 = 1 - \nu + \nu^2$$
$$C_2 = (1 - 2\nu)\,\alpha E$$
$$C_3 = \alpha^2\,E^2$$

For this portion of the analysis (modified plane strain), it will be assumed that the material is elastic-perfectly plastic. It should be noted that this assumption was made for convenience in that it eliminated time consuming code alteration to incorporate a thermo-plastic hardening relationship. Also, since this is primarily a scoping investigation, the elastic-perfectly plastic assumption will give adequate results. Therefore, when the material yields the σ_x-stress can be determined from (4) as follows

$$\sigma_x = \frac{-\,C_2 T \pm \sqrt{(C_2 T)^2 - 4\,C_1(C_3 T^2 - \sigma_o^2)}}{2C_1} \tag{5}$$

The σ_x-stress can be determined from eq. (5) as long as the quantity under the square root sign is positive. This quantity will be positive as long as

$$\sigma_o^2 > \frac{3C_3\,T^2}{4C_4} \tag{6}$$

4. Preliminary Results and Discussion

Preliminary results have been obtained using the above models. The first set of results were obtained using the STRAW code with the plane stress, beam elements. The heated flat is subjected to the three different temperature gradients listed in Table II. The unheated flats are at a constant duct temperature of 1000°F. The deformation of the hexcan wall is found to be as follows: the heated flat (AB) expands, moves upward, and bows. An examination of the displacements for the 540°F temperature gradient indicates that the midflat displacement (point A) in the vertical direction was 0.042 in. while the corner displacement (point B) was 0.026 in. The horizontal displacement of the corner was 0.003 in.

The stress distribution through the hexcan wall at point A is shown in fig. 6. Both the outside and inside regions contain a yield zone, that is, a zone in which the stress has exceeded the initial yield value. It should be noted, however, that the outside plastic zone is larger than the inside zone, and that the stress magnitudes are different. This is to be expected, because the outer zone, being at a higher temperature, has a lower yield stress, hence yielding will occur at a lower stress level. The surface strain of the hexcan along the heated flat was approximately uniform at a value of 0.142 percent.

A comparison between midflat displacements and outer surface strains at point A for the three temperature gradients considered is presented in Table III. The heated flat remained elastic for case 1 (ΔT=270°) and became partially plastic for cases 2 and 3. The unheated flats remained elastic for all cases. A comparison of the strains and displacements under the 540°F and 810°F thermal gradients shows that the larger gradient produces a larger strain but a smaller displacement. This apparent contradiction is explained by examining the mechanisms involved.

The duct may be divided into two parts: a thermally loaded part, flat AB, and the elastic constraint, flats BC, CD, and DE. When the outside surface of flat AB is heated it will tend to bend; the higher the temperature gradient the larger the bending. The elastic constraint resists the bending and the assembly reaches equilibrium when the elastic forces equal the thermal loading. A qualitative examination of the temperature dependent stress-strain curves (fig. 5) indicates the following: (1) the yield stress decreases with increasing temperatures and (2) for a given strain in the plastic range, say ε^* (fig. 5), the corresponding stress decreases with increasing temperature. In effect, the material becomes softer with increasing temperature. Therefore, the elastic unheated flats resist the deformation of the thermally loaded flat to a larger degree at the higher temperatures. For this reason, the midflat deflection is smaller for case 3 than for case 2.

The above results were obtained using a plane-stress beam-type element. A consequence of this is that the predicted strains will tend to be too low. In order to account for a two-dimensional state of stress, such as that existing in a hexcan, the STRAW code was modified as previously explained to approximately represent a state of plane strain. As can be seen from the analysis (eq. 6), there is a limit to the maximum temperature which can be tolerated without axial strains; at this temperature bulging or wrinkling would probably take place if the flat were perfectly confined. For some of the yield strengths indicated in Table I, the maximum plane strain compatible temperatures are presented in Table IV.

In order to properly study the wrinkling problem it is necessary to analyze the heated flat as a two-dimensional configuration in a three-dimension space. To accomplish this, SADCAT was used. However, at the time of this writing, final results from this code are not available. It is, however, anticipated that these results will be available for presentation at the 3rd SMiRT Conference.

References

[1] BELYTSCHKO, T., KENNEDY, J. M., MARCHERTAS, A., "Dynamic Response of Fast-Reactor Core Subassemblies," Nucl. Eng. Design 28, 31-41 (1974).

[2] CRAWFORD, R. M., MARR, W. W., PADILLA, A., WANG, P. Y., LMFBR Subassembly Boundary Integrity: An Interim Report, ANL Report (to be published).

[3] SCHOEBERLE, D. F., KENNEDY, J. M., and BELYTSCHKO, T. B., Implicit Temporal Integration for Long-duration Accidents in a Structural Response Code -- STRAW, ANL-8136 (October 1974).

[4] MARCHERTAS, A. H., and BELYTSCHKO, T. B., Nonlinear Finite-Element Formulation for Transient Analysis of Three-dimensional Thin Structures, ANL-8104 (June 1974).

[5] ZIENKIEWICZ, O. C., The Finite Element Method in Engineering Science, Mc Graw-Hill Publishing Co., London, (1971).

[6] "Steels for Elevated Temperature Service," United States Steel (1965).

TABLE I

Material Property Data

Temperature (°F)	Young's Modulus (10^6 psi)	Temperature (°F)	0.2% Offset Yield Stress (10^3 psi)
1000	22.5	1100	20.5
1200	21.2	1300	19.5
1400	19.6	1500	18.5
1500	18.0	1700	10.5
2000	9.5*	1900	4.5
		2100	2.3
		2300	1.3

*Extrapolated value

TABLE II

Heated Flat Temperatures

Case	ΔT (°F)	T_{inside} (°F)	$T_{outside}$ (°F)
1	270	1080	1350
2	540	1160	1700
3	810	1240	2050

TABLE III

Midflat Displacements and Outer Surface Strain at Point A

Case	ΔT(°F)	U_x (in.)	ε
1	270	.0238	-.00056
2	540	.0417	-.00143
3	810	.0388	-.00439

TABLE IV

Maximum Temperature Difference for Various Yield Strengths

Yield Strength (psi)	Max. Temperature Difference* (°F)
10,000	50
20,000	100
60,000	300

*Reference temperature = 1000°F

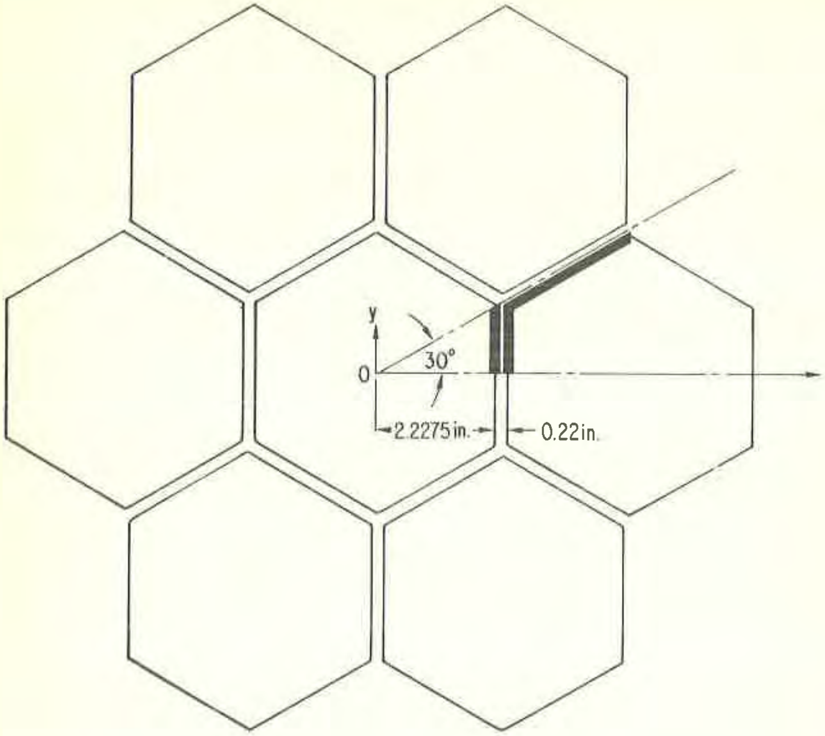

Fig. 1 Subassembly cross-sectional view

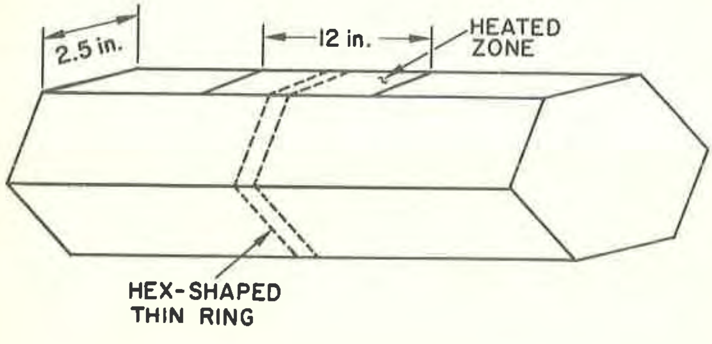

Fig. 2 Thermally loaded hexcan

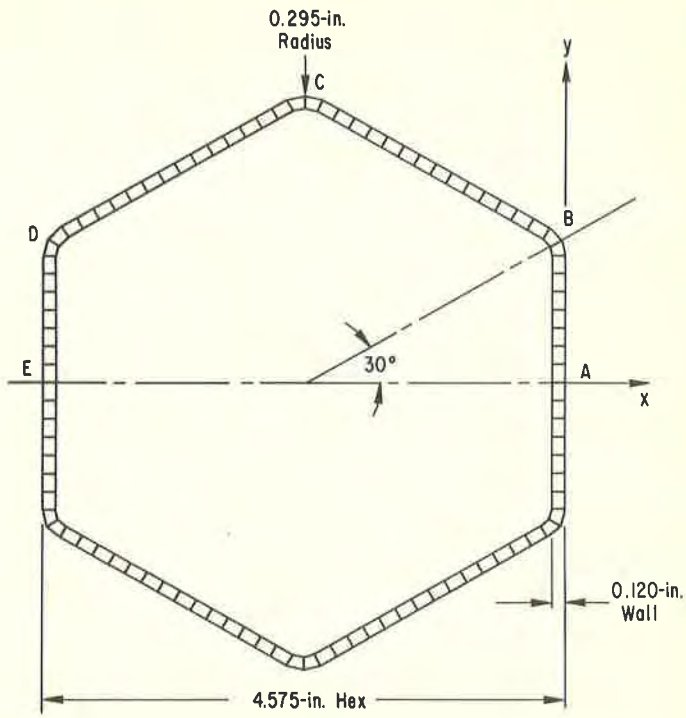

Fig. 3 Finite element model (STRAW)

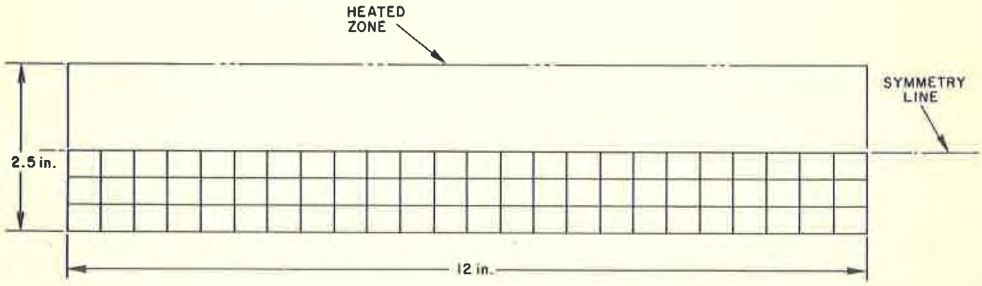

Fig. 4 Finite element model (SADCAT)

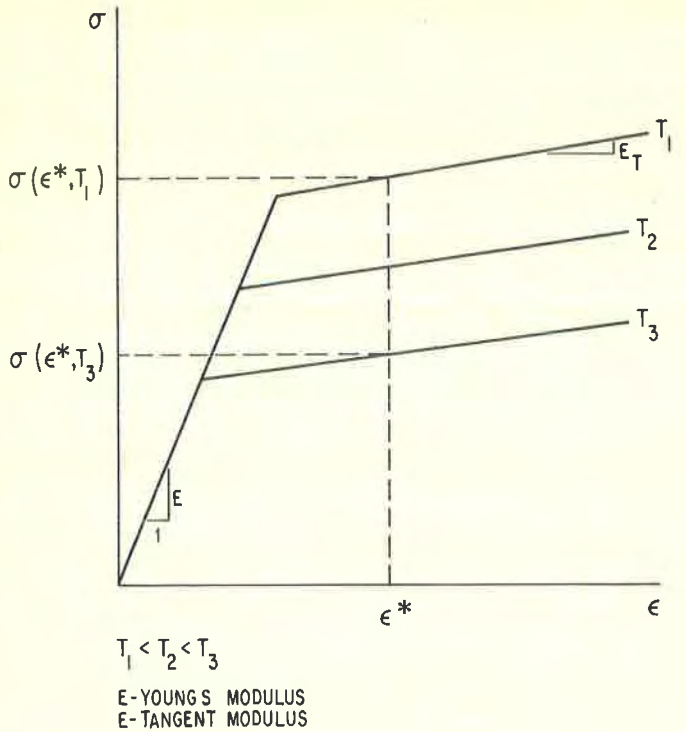

Fig. 5 Temperature dependent stress-strain curve

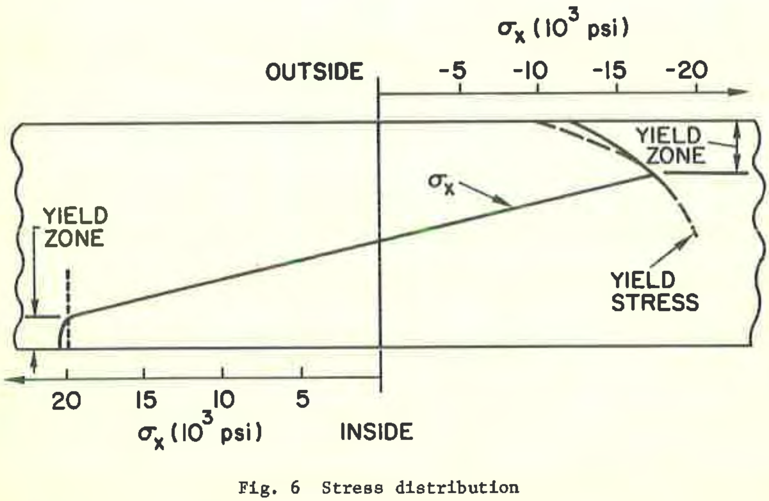

Fig. 6 Stress distribution